Output-based error estimation and mesh adaptation for variational multiscale methods

Brian N. Granzow[1,*], Mark S. Shephard[1], Assad A. Oberai[1]

Scientific Computation Research Center
Rensselaer Polytechnic Institute
110 8th Street
Troy, NY 12180

Abstract

Duality-based approaches to estimate errors for functional output quantities require the solution of an auxiliary dual problem. This dual solution must be approximated in a richer function space than the one used for the original problem of interest. A novel strategy for dual enrichment is proposed based on variational multiscale (VMS) methods and an error representation for output quantities for VMS methods is derived. An implicit error estimate based on the derived error representation is compared to a recently developed explicit error estimate for VMS methods. It is shown that while both estimates are identical with respect to calculating the total output error, the newly derived estimate provides superior local indicators for use in driving mesh adaptivity.

Keywords: a posteriori, error estimation, mesh adapatation, variational multiscale

1. Introduction and motivation

Stabilized finite element methods have been used to effectively solve a wide variety of problems where standard Galerkin methods are known to be unstable. Among these problems are the advective-diffusive equations [12, 18], Stokes flow [17, 4], and the Navier-Stokes equations [7, 11, 26]. The variational multiscale (VMS) method, as developed by Hughes et al. [16, 19], provides a systematic approach to derive a stabilized finite element method. From a high level, the VMS approach decomposes the solution u to a partial differential equation (PDE) into *coarse-scale* components $\overline{u}$ and *fine-scale* components u', where the fine-scale solution is represented or approximated analytically.

A posteriori error estimation is a common tool to assess the accuracy and reliability of a finite element solution [1]. In the original developments of the VMS method, it was suggested that approximations to the fine-scale solution $u' = u - \overline{u}$ could be used to derive *a posteriori* error estimates [16]. Since then, numerous studies have utilized VMS techniques in the context of *a posteriori* error estimation. Hauke et al. [13, 15] investigated using the fine-scale solution as an explicit error estimator in the context of advective transport problems. Masud et al. [24] derived explicit and implicit error estimates for the global discretization error for a mixed form of nearly incompressible elasticity, and then later extended these techniques to nonlinear elasticity formulations [23]. Larson and Målqvist [21] investigated approximating the fine-scale solution via local patch-wise problems, and derived an *a posteriori* error estimate for the solution in the energy norm for use in an adaptive finite element method.

Traditional *a posteriori* error estimates attempt to bound the error in a given norm. More recently developed duality-based *a posteriori* error estimates [10] seek to approximate the error in an output quantity that can be expressed as a functional $J(u)$. For example, outputs corresponding to the lift or drag over an

*Corresponding author, brian.granzow@gmail.com

airfoil may be of primary interest for a numerical study. In general, output-based error estimates based on duality techniques require the solution of an auxiliary *dual problem*. In contrast, the original PDE of interest is referred to as the *primal problem*. Using the solution z to the dual problem, output error estimates are written, in part, as the product of two terms [5, 3]. The first term involves the residual $\mathcal{R}u^h$ of the primal PDE evaluated at the finite element solution. The second term, typically referred to as the weighting term, involves the difference $z - I^h z$ between the exact dual solution and the nodal interpolant of the exact dual solution onto the finite element space used to approximate the primal problem.

The exact dual z solution is generally unknown, and thus must be approximated to obtain functional error estimates. Note that if the dual solution is approximated in the same finite element space as used for the primal problem, then the weighting term in the output error estimate is identically zero. Thus some form of enrichment to the dual solution is required. Several enrichment procedures are commonly used. One approach is to approximate the exact dual solution in a globally richer finite element space than the one used for the primal problem. Another approach involves solving the dual problem using the same finite element space as used for the primal problem and enriching the dual solution via projection. Yet another approach involves using *a priori* estimates to bound the interpolation error in the dual solution.

In this paper we propose a novel strategy for output-based error estimation, whereby the dual solution is enriched by the *fine-scale dual solution* z' using VMS techniques. This is achieved by the introduction of a general representation $\mathcal{E}_2$ for functional errors in VMS methods. Using this general representation, we introduce simple approximations to the fine and coarse scale solutions for both the primal and dual problems to derive an error estimate η_2.

We then seek to demonstrate the utility of this error representation in adaptive finite elements. This is achieved in part by comparison to a recently proposed explicit output-based error representation $\mathcal{E}_1$ that utilizes VMS techniques to entirely circumvent the solution of an auxiliary dual problem [14]. We prove that error estimates $\eta_1 \approx \mathcal{E}_1$ and $\eta_2 \approx \mathcal{E}_2$ based on this explicit error representation and the newly proposed VMS technique, respectively, are identical. However, we demonstrate that localization of the explicit error estimate η_1 is insufficient to drive mesh adaptation for *local* output quantities, whereas the estimate η_2 performs well.

The remainder of this paper is structured as follows. We begin by presenting a review of the derivation of a VMS method for an abstract Dirichlet primal problem. Then we introduce simple approximations to the fine-scale solution u' and the coarse-scale solution $\overline{u}$ to obtain a computable numerical subgrid method for the primal problem. Next, we introduce an auxiliary dual problem to relate the output $J(u)$ to the primal problem. We then derive a VMS and subgrid method for the dual problem. Using the VMS methods for the primal and dual problems, we derive a general expression $\mathcal{E}_2$ for representing output errors in VMS methods, as well as the previously proposed error representation $\mathcal{E}_1$. Then, utilizing the approximations made for the primal and dual subgrid models, we derive error estimates $\eta_1 \approx \mathcal{E}_1$ and $\eta_2 \approx \mathcal{E}_2$ and demonstrate that these two quantities are identical. Next, we discuss the localization of these error estimates to element-level error indicators and how these indicators are used to drive mesh adaptation procedures. Then we investigate the effectivity of error estimates η_1 and η_2 for one and two dimensional example problems. We conclude by investigating the ability of the estimates η_1 and η_2 to drive mesh adaptation to accurately compute output quantities $J(u)$.

2. Review of VMS methods

2.1. Model problem

Let $\Omega \subset \mathbb{R}^d$ be an open bounded domain with smooth boundary $\partial\Omega$, where d is the number of spatial dimensions of the domain. Let $\mathcal{V}$ be a Hilbert space equipped with the norm $\|\cdot\|_{\mathcal{V}}$ and inner product $(\cdot,\cdot)_{\mathcal{V}}$ such that $\mathcal{V} = \{u \in H(\Omega) : u|_{\partial\Omega} = 0\}$, where $H(\Omega)$ is a Hilbert space defined over the domain Ω. Let $\mathcal{V}^*$ be the dual space of $\mathcal{V}$ and ${}_{\mathcal{V}}\langle\cdot,\cdot\rangle_{\mathcal{V}^*}$ denote the dual pairing between the two spaces given by ${}_{\mathcal{V}}\langle v, u\rangle_{\mathcal{V}^*} = \int_\Omega vu \,\mathrm{d}\Omega$. Let $\mathcal{L} : \mathcal{V} \to \mathcal{V}^*$ be a linear differential operator. Let $f \in \mathcal{V}^*$ be given data. We

consider the abstract model problem of finding $u \in \mathcal{V}$ such that

$$\begin{cases} \mathcal{L}u = f, & \boldsymbol{x} \in \Omega, \\ u = 0, & \boldsymbol{x} \in \partial\Omega. \end{cases} \tag{1}$$

In Appendix A we discuss extending this model problem to account for non-homogeneous Dirichlet and Neumann boundary conditions.

We define the residual operator $\mathcal{R} : \mathcal{V} \to \mathcal{V}^*$ as $\mathcal{R}u := f - \mathcal{L}u$, and we refer to (1) as the *primal problem*. The equivalent weak form of the primal problem can be stated as: find $u \in \mathcal{V}$ such that

$$ {}_{\mathcal{V}}\langle v, \mathcal{L}u \rangle_{\mathcal{V}^*} = {}_{\mathcal{V}}\langle v, f \rangle_{\mathcal{V}^*} \quad \forall\, v \in \mathcal{V}. \tag{2}$$

2.2. VMS formulation

In this section, we review the foundations of the VMS method, as developed by Hughes et al. [16] and later refined by Hughes and Sangalli [19]. The basis of the method is the introduction of a sum decomposition of the solution u such that $u = \overline{u} + u'$. Here $\overline{u} \in \overline{\mathcal{V}}$ corresponds to the computable *coarse-scale* solution, while $u' \in \mathcal{V}'$ is associated with unresolved *fine-scales* of the solution. Further, it is assumed that the coarse-scale space $\overline{\mathcal{V}}$ and fine-scale space $\mathcal{V}'$ are closed subspaces of $\mathcal{V}$ and that $\overline{\mathcal{V}} \oplus \mathcal{V}' = \mathcal{V}$.

Using this sum decomposition, the weak form of the primal problem can be restated: find $\overline{u} + u' \in \mathcal{V}$ such that

$$ {}_{\mathcal{V}}\langle v, \mathcal{L}(\overline{u} + u') \rangle_{\mathcal{V}^*} = {}_{\mathcal{V}}\langle v, f \rangle_{\mathcal{V}^*} \quad \forall\, v \in \mathcal{V}, \tag{3}$$

which can be split into the two subproblems: find $\overline{u} + u' \in \mathcal{V}$ such that

$$ {}_{\mathcal{V}}\langle \overline{v}, \mathcal{L}\overline{u} \rangle_{\mathcal{V}^*} + {}_{\mathcal{V}}\langle \overline{v}, \mathcal{L}u' \rangle_{\mathcal{V}^*} = {}_{\mathcal{V}}\langle \overline{v}, f \rangle_{\mathcal{V}^*} \quad \forall\, \overline{v} \in \overline{\mathcal{V}}, \tag{4}$$

$$ {}_{\mathcal{V}}\langle v', \mathcal{L}\overline{u} \rangle_{\mathcal{V}^*} + {}_{\mathcal{V}}\langle v', \mathcal{L}u' \rangle_{\mathcal{V}^*} = {}_{\mathcal{V}}\langle v', f \rangle_{\mathcal{V}^*} \quad \forall\, v' \in \mathcal{V}'. \tag{5}$$

The goal of the VMS method is to eliminate the fine-scale solution u' from the first sub-problem (4) by expressing u' in terms of the coarse-scale solution $\overline{u}$. This results in a coarse-scale model involving only $\overline{u}$ that can then be solved numerically. However, the two sub-problems are not currently well-posed in terms of uniqueness. To ensure uniqueness, an optimality condition $\phi(\cdot)$ is chosen, for example $\phi(\cdot) = \|\cdot\|^2_{H^1(\Omega)}$ or $\phi(\cdot) = \|\cdot\|^2_{L^2(\Omega)}$. The problem is then reposed in the optimal context:

$$\begin{aligned} &\min_{\overline{u}} \quad \phi(u - \overline{u}), \\ &\text{s.t.} \quad \begin{cases} \overline{u} \in \overline{\mathcal{V}}, \\ u' \in \mathcal{V}', \\ \mathcal{L}(\overline{u} + u') = f, \end{cases} \end{aligned} \tag{6}$$

The success of Hughes and Sangalli [19] is in showing that this optimality criteria defines a projector $\mathcal{P} : \mathcal{V} \to \overline{\mathcal{V}}$ onto the coarse-scale space such that $\mathcal{P}u' = 0$. Additionally, the projector $\mathcal{P}$ implicitly defines the fine-scale space $\mathcal{V}' = \{v \in \mathcal{V} : \mathcal{P}v = 0\}$. Using this projector, Hughes and Sangalli then show that the fine-scale solution can be analytically represented as:

$$u' = \underbrace{\left(\mathcal{G} - \mathcal{G}\mathcal{P}^T \left(\mathcal{P}\mathcal{G}\mathcal{P}^T\right)^{-1} \mathcal{P}\mathcal{G}\right)}_{\mathcal{G}'} \mathcal{R}\overline{u}, \tag{7}$$

where $\mathcal{G} = \mathcal{L}^{-1}$ is the classical Green's operator and $\mathcal{G}'$ is the so-called *fine-scale Green's operator*. Similarly, the fine-scale solution can be written in terms of the so-called *fine-scale Green's function* $g'(\boldsymbol{x}; \boldsymbol{y})$ as

$$u'(\boldsymbol{y}) = \int_\Omega g'(\boldsymbol{x}; \boldsymbol{y})(\mathcal{R}\overline{u})(\boldsymbol{x}) \, \mathrm{d}\Omega_x, \tag{8}$$

where $g'(\boldsymbol{x};\boldsymbol{y})$ is defined by the operator $\mathcal{G}'$.

Let $\mathcal{L}^*$ be the adjoint operator of $\mathcal{L}$ such that

$$ {}_{\mathcal{V}}\langle v, \mathcal{L}u\rangle_{\mathcal{V}^*} = {}_{\mathcal{V}^*}\langle \mathcal{L}^* v, u\rangle_{\mathcal{V}} \quad \forall\, u, v \in \mathcal{V}. \tag{9} $$

We note that this equation represents the definition of the adjoint operator $\mathcal{L}^*$ and does not place any restriction on $\mathcal{L}$. When $\mathcal{L}$ is self adjoint, we have the identity $\mathcal{L}^* = \mathcal{L}$, otherwise $\mathcal{L}^*$ and $\mathcal{L}$ are different. However, equation (9) holds in either case.

Using the definition of the adjoint (9) and the representation of the fine-scale solution (7), the first sub-problem (4) can be restated as: find $\overline{u} \in \overline{V}$ such that

$$ {}_{\mathcal{V}}\langle \overline{v}, \mathcal{L}\overline{u}\rangle_{\mathcal{V}^*} + {}_{\mathcal{V}^*}\langle \mathcal{L}^*\overline{v}, \mathcal{G}'\mathcal{R}\overline{u}\rangle_{\mathcal{V}} = {}_{\mathcal{V}}\langle \overline{v}, f\rangle_{\mathcal{V}^*} \quad \forall\, \overline{v} \in \overline{\mathcal{V}}. \tag{10} $$

We refer to this equation as the *continuous variational multiscale* formulation of the primal problem. For use in later derivations, we rewrite this formulation as:

$$ {}_{\mathcal{V}^*}\langle \mathcal{L}^*\overline{v}, \mathcal{G}'\mathcal{R}\overline{u}\rangle_{\mathcal{V}} = {}_{\mathcal{V}}\langle \overline{v}, \mathcal{R}\overline{u}\rangle_{\mathcal{V}^*} \quad \forall\, \overline{v} \in \overline{\mathcal{V}}, \tag{11} $$

recalling the definition of the primal residual operator $\mathcal{R}u := f - \mathcal{L}u$.

2.3. Subgrid model

In practice, the continuous VMS model (10) is approximated by a finite element method. We refer to this approximate model as the *subgrid model*, as is common in the literature. The first step in this approximation is to choose the coarse-scale space to be a finite dimensional subspace, that is $\overline{\mathcal{V}} = \mathcal{V}^h$, and partition the domain Ω into n_{el} non-overlapping finite element subdomains Ω^e with boundaries $\partial\Omega^e$ for $e = 1, 2, \ldots, n_{el}$.

Next we note that an exact representation for the fine-scale Green's function $g'(\boldsymbol{x};\boldsymbol{y})$ (and the fine-scale Green's operator $\mathcal{G}'$) is generally not obtainable. Thus, we must introduce an approximation for the fine-scale Green's function to accurately represent the fine-scale solution (8). To this end, we introduce the so-called *element-level Green's function* $g^e(\boldsymbol{x};\boldsymbol{y})$, defined over element interiors as

$$ \begin{cases} \mathcal{L}^* g^e(\boldsymbol{x};\boldsymbol{y}) = \delta(\boldsymbol{x}-\boldsymbol{y}), & \boldsymbol{x} \in \Omega^e, \\ \quad g^e(\boldsymbol{x};\boldsymbol{y}) = 0, & \boldsymbol{x} \in \partial\Omega^e, \end{cases} \tag{12} $$

such that $g'(\boldsymbol{x};\boldsymbol{y}) \approx g^e(\boldsymbol{x};\boldsymbol{y})$.

Note that this approximation assumes that the fine-scale solution u' vanishes on element boundaries $\partial\Omega^e$. Hughes and Sangalli [19] show that, in one spatial dimension, the choice of an H^1 optimality condition $\phi = \|\cdot\|_{H^1}^2$ results in a completely *local* fine-scale Green's function. That is, when $d = 1$, the H^1 optimality condition ensures the equivalence of the fine-scale Green's function $g'(\boldsymbol{x};\boldsymbol{y})$ and the element-level Green's function $g^e(\boldsymbol{x};\boldsymbol{y})$. This result provides justification for approximating the fine-scale Green's function as the element-level Green's function and motivates us to only consider $\phi(\cdot) = \|\cdot\|_{H^1}$ in this work.

As a further simplification, we approximate the element-level Green's function by it's *average* value over the element interior, and denote this value by τ^e, which can be expressed as:

$$ \tau^e = \frac{1}{\operatorname{meas}(\Omega^e)} \int_{\Omega^e} \int_{\Omega^e} g^e(\boldsymbol{x};\boldsymbol{y})\, \mathrm{d}\Omega_x\, \mathrm{d}\Omega_y. \tag{13} $$

We note that more accurate approximations for the element-level Green's function can be made. For instance, Oberai and Pinsky [25] approximate the element-level Green's function by a polynomial scalar function involving *moments* of the element-level Green's function. We leave investigation into this area as a consideration for future work.

With this final approximation, the subgrid model can be written as: find $u^h \in \mathcal{V}^h$ such that

$$ {}_{\mathcal{V}}\big\langle v^h, \mathcal{L}u^h\big\rangle_{\mathcal{V}^*} + {}_{\mathcal{V}^*}\big\langle \mathcal{L}^* v^h, \tau^e \mathcal{R}u^h\big\rangle_{\mathcal{V}}^{\Omega'} = {}_{\mathcal{V}}\big\langle v^h, f\big\rangle_{\mathcal{V}^*} \quad \forall\, v^h \in \mathcal{V}^h, \tag{14} $$

or equivalently as: find $u^h \in \mathcal{V}^h$ such that

$$ {}_{\mathcal{V}^*}\big\langle \mathcal{L}^* v^h, \tau^e \mathcal{R} u^h \big\rangle_{\mathcal{V}}^{\Omega'} = {}_{\mathcal{V}}\big\langle v^h, \mathcal{R} u^h \big\rangle_{\mathcal{V}^*} \quad \forall\, v^h \in \mathcal{V}^h, \tag{15} $$

where we have approximated the fine-scale solution over element interiors as

$$ u'\big|_{\Omega^e} \approx \widetilde{u}'\big|_{\Omega^e} = \tau^e \mathcal{R} u^h. \tag{16} $$

Here ${}_{\mathcal{V}^*}\langle \cdot, \cdot \rangle_{\mathcal{V}}^{\Omega'}$ denotes the 'broken' dual pairing over element interiors given by

$$ {}_{\mathcal{V}^*}\langle u, v \rangle_{\mathcal{V}}^{\Omega'} = \sum_{e=1}^{n_{el}} {}_{\mathcal{V}^*}\langle u, v \rangle_{\mathcal{V}}^{\Omega^e}, \tag{17} $$

where we have denoted the dual pairing over a single element interior as

$$ {}_{\mathcal{V}^*}\langle u, v \rangle_{\mathcal{V}}^{\Omega^e} = \int_{\Omega^e} uv \, \mathrm{d}\Omega. \tag{18} $$

We emphasize that the approximations made to the fine-scale solution imply that the subgrid model (14) is an approximation to the continuous VMS formulation (10), which in turn implies that the subgrid solution u^h is an approximation to the coarse-scale solution $\overline{u}$. With this in mind, we can express the exact solution u as

$$ u = u^h + \widetilde{u}' + \widetilde{u} \tag{19} $$

where $\widetilde{u} = (\overline{u} - u^h) + (u' - \widetilde{u}')$ represents the approximation errors in the coarse and fine-scale solutions.

Remark 1. The finite element method is derived from the weak form of a partial differential equation that has been integrated by parts. Thus instead of the duality pairing used in equation (14) it makes use of the L_2 inner product, and the finite element subgrid model derived from the variational multiscale method is given by:

$$ A(v^h, u^h) + (\mathcal{L}^* v^h, \tau^e \mathcal{R} u^h)_{\Omega'} = l(v^h) \quad \forall\, v \in \mathcal{V}. \tag{20} $$

where $A(\cdot, \cdot)$ is the bilinear form associated with the operator $\mathcal{L}$, $(\cdot, \cdot)_{\Omega'}$ is the broken L_2 inner product defined on element interiors, and $l(\cdot)$ is the linear functional associated with the forcing function f.

3. The dual problem

3.1. Abstract problem

Let $J(u) : \mathcal{V} \to \mathbb{R}$ be a linear functional corresponding to a physically meaningful quantity of interest. We assume that $J(u)$ can be expressed as

$$ J(u) = {}_{\mathcal{V}^*}\langle q, u \rangle_{\mathcal{V}}, \tag{21} $$

where $q \in \mathcal{V}^*$. Following standard duality-based approaches for *a posteriori* error estimation [3, 5, 9, 10] we introduce the *dual problem* : find $z \in \mathcal{V}$ such that

$$ {}_{\mathcal{V}^*}\langle \mathcal{L}^* z, v \rangle_{\mathcal{V}} = {}_{\mathcal{V}^*}\langle q, v \rangle_{\mathcal{V}} \quad \forall\, v \in \mathcal{V}. \tag{22} $$

The equivalent strong form of the dual problem can be written as: find $z \in \mathcal{V}$ such that

$$ \begin{cases} \mathcal{L}^* z = q, & \boldsymbol{x} \in \Omega, \\ \quad z = 0, & \boldsymbol{x} \in \partial\Omega. \end{cases} \tag{23} $$

We define the residual operator $\mathcal{R}^* : \mathcal{V} \to \mathcal{V}^*$ of the dual problem as $\mathcal{R}^* z := q - \mathcal{L}^* z$.

3.2. VMS formulation

If the primal problem necessitates the use of numerical stabilization, it is also likely that solving the dual problem (22) with a Galerkin finite element method will yield spurious oscillations in the dual solution [8]. To prevent non-physical behavior in the dual solution, we also solve the dual problem with a VMS method. Cyr et al. [8] call this approach the *stabilization of the adjoint*. This is in contrast to deriving a dual problem directly from the primal subgrid model (14), which Cyr et al. refer to as the *adjoint of the stabilization*.

Let $\overline{\mathcal{V}}_d$ and $\mathcal{V}'_d$ be closed subspaces of $\mathcal{V}$. Obtaining a VMS formulation for the dual problem proceeds in exactly the same manner as the primal problem. First a sum decomposition of the dual solution z is assumed such that $z = \overline{z} + z'$, where $\overline{z} \in \overline{\mathcal{V}}_d$ and $z' \in \mathcal{V}'_d$. The weak form of the dual problem (22) is then written as two sub-problems, whose solutions are uniquely determined by an optimality condition $\phi_d(\cdot)$ imposed on the coarse-scale solution $\overline{z}$. As with the primal model, we will only consider the H^1 optimality condition $\phi_d(\cdot) = \|\cdot\|^2_{H^1}$. However, we note that one could potentially choose different optimality conditions for both the primal and dual problems. We leave investigation into this area as an open research topic.

The optimality condition defines a projector $\mathcal{P}_d : \mathcal{V} \to \overline{\mathcal{V}}_d$ onto the coarse-scale subspace such that $P_d z' = 0$, and this projector implicitly defines the fine-scale subspace as $\overline{\mathcal{V}}_d = \{v \in \mathcal{V} : \mathcal{P}_d v = 0\}$. If we let $\mathcal{G}_d$ denote the classical Green's operator for the dual problem, such that $\mathcal{G}_d = (\mathcal{L}^*)^{-1}$, then the fine-scale dual solution can be represented as:

$$z' = \underbrace{\left(\mathcal{G}_d - \mathcal{G}_d\mathcal{P}_d^T\left(\mathcal{P}_d\mathcal{G}_d\mathcal{P}_d^T\right)^{-1}\mathcal{P}_d\mathcal{G}_d\right)}_{\mathcal{G}'_d}\mathcal{R}^*\overline{z}, \tag{24}$$

where $\mathcal{G}'_d$ is the *dual fine-scale Green's operator*. Similarly, the fine-scale solution can be written in terms of the *dual fine-scale Green's function*, $g'_d(\boldsymbol{x};\boldsymbol{y})$, as:

$$z'(\boldsymbol{y}) = \int_\Omega g'_d(\boldsymbol{x};\boldsymbol{y})(\mathcal{R}^*\overline{z})(\boldsymbol{x})\,\mathrm{d}\Omega_x, \tag{25}$$

where $g'_d(\boldsymbol{x};\boldsymbol{y})$ is defined by the operator $\mathcal{G}'_d$. Using this representation of the fine-scale dual solution, the *continuous variational multiscale* formulation of the dual problem is stated as: find $\overline{z} \in \overline{\mathcal{V}}_d$ such that

$${}_{\mathcal{V}^*}\langle\mathcal{L}^*\overline{z},\overline{v}\rangle_{\mathcal{V}} + {}_{\mathcal{V}}\langle\mathcal{G}'_d\mathcal{R}^*\overline{z},\mathcal{L}\overline{v}\rangle_{\mathcal{V}^*} = {}_{\mathcal{V}^*}\langle q,\overline{v}\rangle_{\mathcal{V}} \quad \forall\,\overline{z} \in \overline{\mathcal{V}}_d. \tag{26}$$

Recalling the definition of the dual residual operator $\mathcal{R}^* := q - \mathcal{L}^*$, we can rewrite equation (26) as:

$${}_{\mathcal{V}}\langle\mathcal{G}'_d\mathcal{R}^*\overline{z},\mathcal{L}\overline{v}\rangle_{\mathcal{V}^*} = {}_{\mathcal{V}^*}\langle\mathcal{R}^*\overline{z},\overline{v}\rangle_{\mathcal{V}} \quad \forall\,\overline{z} \in \overline{\mathcal{V}}_d. \tag{27}$$

3.3. Subgrid model

To derive a corresponding subgrid model to the VMS formulation of the dual problem (26), we will assume that the coarse-scale spaces for the primal and dual problem are chosen to be the same, such that $\overline{\mathcal{V}} = \overline{\mathcal{V}}_d$. Additionally, we will consider approximations made using the same finite dimensional subspace $\overline{\mathcal{V}} = \mathcal{V}^h$ and discretization as used for the primal subgrid model. We first approximate the dual fine-scale Green's function $g'_d(\boldsymbol{x};\boldsymbol{y})$ using the *dual element-level Green's function*, defined over element interiors as

$$\begin{cases} \mathcal{L}g^e_d(\boldsymbol{x};\boldsymbol{y}) = \delta(\boldsymbol{x}-\boldsymbol{y}), & \boldsymbol{x} \in \Omega^e, \\ g^e_d(\boldsymbol{x};\boldsymbol{y}) = 0, & \boldsymbol{x} \in \partial\Omega^e, \end{cases} \tag{28}$$

such that $g'_d(\boldsymbol{x};\boldsymbol{y}) \approx g^e_d(\boldsymbol{x};\boldsymbol{y})$.

We further approximate the fine-scale dual solution z' by writing it as the product of a scalar function τ^e_d times the dual residual operating on the coarse-scale solution. The scalar function is given as:

$$\tau^e_d = \frac{1}{\mathrm{meas}(\Omega^e)}\int_{\Omega^e}\int_{\Omega^e} g^e_d(\boldsymbol{x};\boldsymbol{y})\,\mathrm{d}\Omega_x\,\mathrm{d}\Omega_y. \tag{29}$$

The dual subgrid model can then be written as: find $z^h \in \mathcal{V}^h$ such that

$$ {}_{\mathcal{V}^*}\langle \mathcal{L}^* z^h, v^h \rangle_{\mathcal{V}} + {}_{\mathcal{V}}\langle \tau_d^e \mathcal{R}^* z^h, \mathcal{L} v^h \rangle_{\mathcal{V}^*}^{\Omega'} = {}_{\mathcal{V}^*}\langle q, v^h \rangle_{\mathcal{V}} \quad \forall\, v^h \in \mathcal{V}^h, \tag{30} $$

or equivalently as: find $z^h \in \mathcal{V}^h$ such that

$$ {}_{\mathcal{V}}\langle \tau_d^e \mathcal{R}^* z^h, \mathcal{L} v^h \rangle_{\mathcal{V}^*}^{\Omega'} = {}_{\mathcal{V}^*}\langle \mathcal{R}^* z^h, v^h \rangle_{\mathcal{V}} \quad \forall\, v^h \in \mathcal{V}^h, \tag{31} $$

where we have approximated the fine-scale dual solution over element interiors as

$$ z'\big|_{\Omega^e} \approx \widetilde{z}'\big|_{\Omega^e} = \tau_d^e \mathcal{R}^* z^h. \tag{32} $$

We note that the exact dual solution can be expressed as the sum

$$ z = z^h + \widetilde{z}' + \widetilde{z}, \tag{33} $$

where $\widetilde{z} = (\overline{z} - z^h) + (z' - \widetilde{z}')$ represents the approximation errors in the coarse and fine-scale solutions.

Remark 2. The finite element version of the dual subgrid model corresponding to equation (30) is written using the L_2 inner product as:

$$ A(z^h, v^h) + (\tau_d^e \mathcal{R}^* z^h, \mathcal{L} v^h)_{\Omega'} = J(v^h) \quad \forall\, v \in \mathcal{V}^h, \tag{34} $$

where $A(\cdot,\cdot)$ is the bilinear form associated with the operator $\mathcal{L}$, and $(\cdot,\cdot)_{\Omega'}$ is the broken L_2 inner product defined on element interiors.

4. Error estimation

In this section, we develop a general framework for output-based error estimation in VMS methods. We first develop two error representations for output quantities in the continuous VMS setting. Next, we discuss the role of the approximations made in both the primal and dual subgrid models. Finally, we introduce two error estimates for output quantities. We prove that the error estimates are identical. However, we demonstrate the superiority of one estimate over the other in the context of error localization needed to drive mesh adaptation.

4.1. Continuous VMS error representations

Proposition 1. *For any solution $u = u' + \overline{u}$ to the continuous VMS formulation* (10)*, we have the error representation*

$$ \mathcal{E}_1 = J(u) - J(\overline{u}) = J(u') \tag{35} $$

Proof. The result follows directly from the linearity of $J(\cdot)$ and the sum decomposition $u = u' + \overline{u}$. □

This error representation is used by Hauke and Fuster [14] to derive an explicit *a posteriori* error estimate for output quantities. The error estimate only involves an approximation $\widetilde{u}'$ to the fine-scale solution u' and completely avoids the solution of a dual problem. However, when q is chosen to be a *local* forcing function for the dual problem (e.g. a function which is non-zero only over a subdomain of the total domain), error estimates derived from this representation fail to provide useful information when they are localized to the element level. Such error localization is critical to drive mesh adaptation and is discussed in detail later.

Proposition 2. *For any solutions $u = u' + \overline{u}$ to the continuous VMS formulation* (10) *and $z = z' + \overline{z}$ to the continuous dual VMS formulation* (26)*, we have the error representation*

$$ \mathcal{E}_2 = J(u) - J(\overline{u}) = {}_{\mathcal{V}}\langle \mathcal{G}_d' \mathcal{R}^* \overline{z}, \mathcal{R}\overline{u} \rangle_{\mathcal{V}^*} + {}_{\mathcal{V}^*}\langle \mathcal{L}^* \overline{z}, \mathcal{G}' \mathcal{R} \overline{u} \rangle_{\mathcal{V}} \tag{36} $$

Proof.

$$\begin{aligned}
J(u) - J(\overline{u}) &= {}_{\mathcal{V}^*}\langle q, u\rangle_{\mathcal{V}} - {}_{\mathcal{V}^*}\langle q, \overline{u}\rangle_{\mathcal{V}} && \text{by (21)} \\
&= {}_{\mathcal{V}^*}\langle \mathcal{L}^* z, u\rangle_{\mathcal{V}} - {}_{\mathcal{V}^*}\langle \mathcal{L}^* z, \overline{u}\rangle_{\mathcal{V}} && \text{by (22)} \\
&= {}_{\mathcal{V}}\langle z, \mathcal{L}u\rangle_{\mathcal{V}^*} - {}_{\mathcal{V}}\langle z, \mathcal{L}\overline{u}\rangle_{\mathcal{V}^*} && \text{by (9)} \\
&= {}_{\mathcal{V}}\langle z, f\rangle_{\mathcal{V}^*} - {}_{\mathcal{V}}\langle z, \mathcal{L}\overline{u}\rangle_{\mathcal{V}^*} && \text{by (2)} \\
&= {}_{\mathcal{V}}\langle z, \mathcal{R}\overline{u}\rangle_{\mathcal{V}^*} && \text{by definition, linearity} \\
&= {}_{\mathcal{V}}\langle z', \mathcal{R}\overline{u}\rangle_{\mathcal{V}^*} + {}_{\mathcal{V}}\langle \overline{z}, \mathcal{R}\overline{u}\rangle_{\mathcal{V}^*} && \text{by definition, linearity} \\
&= {}_{\mathcal{V}}\langle z', \mathcal{R}\overline{u}\rangle_{\mathcal{V}^*} + {}_{\mathcal{V}^*}\langle \mathcal{L}^*\overline{z}, \mathcal{G}'\mathcal{R}\overline{u}\rangle_{\mathcal{V}} && \text{by (11)} \\
&= {}_{\mathcal{V}}\langle \mathcal{G}_d'\mathcal{R}^*\overline{z}, \mathcal{R}\overline{u}\rangle_{\mathcal{V}^*} + {}_{\mathcal{V}^*}\langle \mathcal{L}^*\overline{z}, \mathcal{G}'\mathcal{R}\overline{u}\rangle_{\mathcal{V}} && \text{by (24)}
\end{aligned}$$

□

This error representation suggests a general approach to output-based error estimation for VMS methods, where the only approximation made to this point is that the coarse-scale subspace for the primal and dual problems are equal, such that $\overline{\mathcal{V}} = \overline{\mathcal{V}}_d$. To derive computable error estimates, exact representations or approximations must be known for the fine-scale Green's operators and the coarse-scale solutions for both the primal and dual problems.

4.2. Subgrid model error representations

We now derive error representations that arise by introducing the approximations made in the primal and dual subgrid models.

Proposition 3. *For any solutions u to the primal model* (2) *and u^h to the primal subgrid model* (14)*, we have the error representation*

$$\hat{\mathcal{E}}_1 = J(u) - J(u^h) = {}_{\mathcal{V}^*}\big\langle q, \tau^e \mathcal{R} u^h \big\rangle_{\mathcal{V}}^{\Omega'} + {}_{\mathcal{V}^*}\langle q, \widetilde{u}\rangle_{\mathcal{V}} \tag{37}$$

Proof.

$$\begin{aligned}
J(u) - J(u^h) &= {}_{\mathcal{V}^*}\langle q, u\rangle_{\mathcal{V}} - {}_{\mathcal{V}^*}\big\langle q, u^h\big\rangle_{\mathcal{V}} && \text{by (21)} \\
&= {}_{\mathcal{V}^*}\big\langle q, u - u^h\big\rangle_{\mathcal{V}} && \text{by linearity} \\
&= {}_{\mathcal{V}^*}\langle q, \widetilde{u}' + \widetilde{u}\rangle_{\mathcal{V}} && \text{by (19)} \\
&= {}_{\mathcal{V}^*}\langle q, \widetilde{u}'\rangle_{\mathcal{V}}^{\Omega'} + {}_{\mathcal{V}^*}\langle q, \widetilde{u}\rangle_{\mathcal{V}} && \text{by linearity} \\
&= {}_{\mathcal{V}^*}\big\langle q, \tau^e \mathcal{R} u^h\big\rangle_{\mathcal{V}}^{\Omega'} + {}_{\mathcal{V}^*}\langle q, \widetilde{u}\rangle_{\mathcal{V}} && \text{by (16)}
\end{aligned}$$

□

Proposition 4. *For any solutions u to the primal model* (2)*, z to the dual model* (22)*, u^h to the primal subgrid model* (14) *and z^h to the dual subgrid model* (30)*, we have the error representation*

$$\hat{\mathcal{E}}_2 = J(u) - J(u^h) = {}_{\mathcal{V}}\big\langle \tau_d^e \mathcal{R}^* z^h, \mathcal{R} u^h\big\rangle_{\mathcal{V}^*}^{\Omega'} + {}_{\mathcal{V}^*}\big\langle \mathcal{L}^* z^h, \tau^e \mathcal{R} u^h\big\rangle_{\mathcal{V}}^{\Omega'} + {}_{\mathcal{V}}\big\langle \widetilde{z}, \mathcal{R} u^h\big\rangle_{\mathcal{V}^*} \tag{38}$$

Proof.

$$
\begin{aligned}
J(u) - J(u^h) &= {}_{\mathcal{V}^*}\langle q, u\rangle_{\mathcal{V}} - {}_{\mathcal{V}^*}\langle q, u^h\rangle_{\mathcal{V}} && \text{by (21)}\\
&= {}_{\mathcal{V}^*}\langle \mathcal{L}^* z, u\rangle_{\mathcal{V}} - {}_{\mathcal{V}^*}\langle \mathcal{L}^* z, u^h\rangle_{\mathcal{V}} && \text{by (22)}\\
&= {}_{\mathcal{V}}\langle z, \mathcal{L}u\rangle_{\mathcal{V}^*} - {}_{\mathcal{V}}\langle z, \mathcal{L}u^h\rangle_{\mathcal{V}^*} && \text{by (9)}\\
&= {}_{\mathcal{V}}\langle z, f\rangle_{\mathcal{V}^*} - {}_{\mathcal{V}}\langle z, \mathcal{L}u^h\rangle_{\mathcal{V}^*} && \text{by (2)}\\
&= {}_{\mathcal{V}}\big\langle z, \mathcal{R}u^h\big\rangle_{\mathcal{V}^*} && \text{by definition}\\
&= {}_{\mathcal{V}}\big\langle z, \mathcal{R}u^h\big\rangle_{\mathcal{V}^*} - {}_{\mathcal{V}}\big\langle z^h, \mathcal{R}u^h\big\rangle_{\mathcal{V}^*} + {}_{\mathcal{V}^*}\big\langle \mathcal{L}^* z^h, \tau^e \mathcal{R}u^h\big\rangle_{\mathcal{V}}^{\Omega'} && \text{by (15)}\\
&= {}_{\mathcal{V}}\big\langle z - z^h, \mathcal{R}u^h\big\rangle_{\mathcal{V}^*} + {}_{\mathcal{V}^*}\big\langle \mathcal{L}^* z^h, \tau^e \mathcal{R}u^h\big\rangle_{\mathcal{V}}^{\Omega'} && \text{by linearity}\\
&= {}_{\mathcal{V}}\big\langle \widetilde{z}' + \widetilde{z}, \mathcal{R}u^h\big\rangle_{\mathcal{V}^*} + {}_{\mathcal{V}^*}\big\langle \mathcal{L}^* z^h, \tau^e \mathcal{R}u^h\big\rangle_{\mathcal{V}}^{\Omega'} && \text{by (33)}\\
&= {}_{\mathcal{V}}\big\langle \widetilde{z}', \mathcal{R}u^h\big\rangle_{\mathcal{V}^*}^{\Omega'} + {}_{\mathcal{V}^*}\big\langle \mathcal{L}^* z^h, \tau^e \mathcal{R}u^h\big\rangle_{\mathcal{V}}^{\Omega'} + {}_{\mathcal{V}}\big\langle \widetilde{z}, \mathcal{R}u^h\big\rangle_{\mathcal{V}^*} && \text{by linearity}\\
&= {}_{\mathcal{V}}\big\langle \tau_d^e \mathcal{R}^* z^h, \mathcal{R}u^h\big\rangle_{\mathcal{V}^*}^{\Omega'} + {}_{\mathcal{V}^*}\big\langle \mathcal{L}^* z^h, \tau^e \mathcal{R}u^h\big\rangle_{\mathcal{V}}^{\Omega'} + {}_{\mathcal{V}}\big\langle \widetilde{z}, \mathcal{R}u^h\big\rangle_{\mathcal{V}^*} && \text{by (32)}
\end{aligned}
$$

□

4.3. Subgrid model error estimates

In general, the approximation errors $\widetilde{u}$ and $\widetilde{z}$ are unknown. This suggests the error *estimates* $\eta_1 \approx \hat{\mathcal{E}}_1$ and $\eta_2 \approx \hat{\mathcal{E}}_2$ that are obtained by setting $\widetilde{u} = 0$ in (37) and $\widetilde{z} = 0$ in (38), and are given below:

$$\eta_1 = {}_{\mathcal{V}^*}\big\langle q, \tau^e \mathcal{R}u^h\big\rangle_{\mathcal{V}}^{\Omega'} \tag{39}$$

$$\eta_2 = {}_{\mathcal{V}}\big\langle \tau_d^e \mathcal{R}^* z^h, \mathcal{R}u^h\big\rangle_{\mathcal{V}^*}^{\Omega'} + {}_{\mathcal{V}^*}\big\langle \mathcal{L}^* z^h, \tau^e \mathcal{R}u^h\big\rangle_{\mathcal{V}}^{\Omega'} \tag{40}$$

Proposition 5. *For any solutions u^h to the primal subgrid model* (14) *and z^h to the dual subgrid model* (30) *the error estimates η_1 and η_2 are identical.*

Proof. Note that if the stabilization parameters τ^e and τ_d^e for the primal and dual problems are equal, we obtain the desired result since

$$
\begin{aligned}
\eta_2 &= {}_{\mathcal{V}}\big\langle \tau_d^e \mathcal{R}^* z^h, \mathcal{R}u^h\big\rangle_{\mathcal{V}^*}^{\Omega'} + {}_{\mathcal{V}^*}\big\langle \mathcal{L}^* z^h, \tau^e \mathcal{R}u^h\big\rangle_{\mathcal{V}}^{\Omega'}\\
&= {}_{\mathcal{V}^*}\big\langle \mathcal{R}^* z^h, \tau^e \mathcal{R}u^h\big\rangle_{\mathcal{V}}^{\Omega'} + {}_{\mathcal{V}^*}\big\langle \mathcal{L}^* z^h, \tau^e \mathcal{R}u^h\big\rangle_{\mathcal{V}}^{\Omega'} && \text{by assumption}\\
&= {}_{\mathcal{V}^*}\big\langle \mathcal{R}^* z^h + \mathcal{L}^* z^h, \tau^e \mathcal{R}u^h\big\rangle_{\mathcal{V}}^{\Omega'} && \text{by linearity}\\
&= {}_{\mathcal{V}^*}\big\langle q, \tau^e \mathcal{R}u^h\big\rangle_{\mathcal{V}}^{\Omega'} && \text{by definition}\\
&= \eta_1
\end{aligned}
$$

Using the given definitions (13) and (29), we note that a sufficient condition for the equality $\tau^e = \tau_d^e$ is: $g^e(\boldsymbol{x};\boldsymbol{y}) = g_d^e(\boldsymbol{y};\boldsymbol{x})$. This is verified via the following argument:

$$
\begin{aligned}
&\mathcal{L}^* g^e(\boldsymbol{x};\boldsymbol{y}) = \delta(\boldsymbol{x}-\boldsymbol{y}) && \text{by (12)}\\
\implies &\int_{\Omega^e} g_d^e(\boldsymbol{x};\boldsymbol{z}) \mathcal{L}^* g^e(\boldsymbol{x};\boldsymbol{y})\,\mathrm{d}\Omega = \int_{\Omega^e} g_d^e(\boldsymbol{x};\boldsymbol{z})\delta(\boldsymbol{x}-\boldsymbol{y})\,\mathrm{d}\Omega\\
\implies &\int_{\Omega^e} \mathcal{L} g_d^e(\boldsymbol{x};\boldsymbol{z}) g^e(\boldsymbol{x};\boldsymbol{y})\,\mathrm{d}\Omega = \int_{\Omega^e} g_d^e(\boldsymbol{x};\boldsymbol{z})\delta(\boldsymbol{x}-\boldsymbol{y})\,\mathrm{d}\Omega\\
\implies &\int_{\Omega^e} \delta(\boldsymbol{x}-\boldsymbol{z}) g^e(\boldsymbol{x};\boldsymbol{y})\,\mathrm{d}\Omega = \int_{\Omega^e} g_d^e(\boldsymbol{x};\boldsymbol{z})\delta(\boldsymbol{x}-\boldsymbol{y})\,\mathrm{d}\Omega && \text{by (28)}\\
&\implies g^e(\boldsymbol{z};\boldsymbol{y}) = g_d^e(\boldsymbol{y};\boldsymbol{z})
\end{aligned}
$$

Here we remark that the identity (9) holds for arbitrary smooth domains Ω and for a function space $\mathcal{V}$ whose members vanish on the boundary $\partial\Omega$. As such, we employ the element-level identity:

$$ {}_{\mathcal{V}}\langle v, \mathcal{L}u\rangle_{\mathcal{V}^*}^{\Omega^e} = {}_{\mathcal{V}^*}\langle \mathcal{L}^* v, u\rangle_{\mathcal{V}}^{\Omega^e} \quad \forall u, v \in \mathcal{V}^e \tag{41} $$

to derive the third equality above, where $\mathcal{V}^e = \{u \in \mathcal{V} : u = 0 \text{ on } \partial\Omega^e\}$. □

4.4. Error localization

We now demonstrate that even though η_1 and η_2 are identical global error estimates, their localization to element-level error estimates is very different. This localization yields positive values at the element level called *error indicators* which are necessary to drive mesh adaptation. We compute error indicators by bounding the two error estimates η_1 and η_2 from above using the triangle inequality, such that:

$$ |\eta_1| \leq \sum_{e=1}^{n_{el}} \eta_1^e, \tag{42} $$

and

$$ |\eta_2| \leq \sum_{e=1}^{n_{el}} \eta_2^e. \tag{43} $$

Here the error indicator for the error estimate η_1 is given as

$$ \eta_1^e = |\, {}_{\mathcal{V}^*}\big\langle q, \tau^e \mathcal{R}u^h \big\rangle_{\mathcal{V}}^{\Omega^e} \,|, \tag{44} $$

and the error indicator for the error estimate η_2 is given as

$$ \eta_2^e = |\, {}_{\mathcal{V}}\big\langle \tau_d^e \mathcal{R}^* z^h, \mathcal{R}u^h \big\rangle_{\mathcal{V}^*}^{\Omega^e} \,| + |\, {}_{\mathcal{V}^*}\big\langle \mathcal{L}^* z^h, \tau^e \mathcal{R}u^h \big\rangle_{\mathcal{V}}^{\Omega^e} \,| \tag{45} $$

Note that the indicator η_1^e is only non-zero over elements for which the dual forcing function $q|_{\Omega^e}$ is non-zero. This indicates that only elements for which $q|_\Omega \neq 0$ provide contributions to the error $J(u) - J(u^h)$, which is generally not true. As a thought experiment, consider an advective problem for which the dual forcing function q is defined to be 1 over some subdomain $\Omega^s \subset \Omega$ and 0 elsewhere. Any discretization errors introduced upstream of the subdomain Ω^s will be propagated via advection to the subdomain itself, thus affecting the accuracy of the computed output quantity. However, the indicator η_1^e will indicate that the elements upstream of the subdomain provide no contributions to the output error, as these elements are located outside of the subdomain Ω^s, whereas this would not be the case for η_2^e.

5. Mesh adaptation

Mesh adaptation provides a means to modify the spatial discretization of a PDE to obtain greater solution accuracy with a given amount of computing power. Presently, we make use of conformal unstructured local mesh modification that performs sequences of edge splits, swaps, and collapses [2] [22] using the PUMI [20] software suite. Mesh adaptation is driven by the concept of a *mesh size field*, which defines element edge lengths at all locations in the mesh. The mesh size field is determined by the localized error indicators to perform mesh refinement in areas that strongly contribute to the error and perform mesh coarsening in areas that do not strongly contribute to the error.

5.1. Size field specification

Let N be a desired target number of mesh elements. Let η^e denote a computed element-level error indicator defined for all $e = 1, 2, \ldots, n_{el}$. Let p be the expected polynomial order of convergence for a chosen finite element method. Following Boussetta et al. [6], we utilize a size field specification that aims to provide an output adapted mesh with N elements. First, we define the global quantity G as

$$G = \sum_{e}^{n_{el}} (\eta^e)^{\frac{2d}{2p+d}} . \tag{46}$$

Once G has been computed, new element-level sizes h^e_{new} are determined by scaling the previous element size h_e according to the formula

$$h^e_{\text{new}} = \left(\frac{G}{N}\right)^{\frac{1}{d}} (\eta^e)^{\frac{-2}{2p+d}} \, h^e \tag{47}$$

Finally, to prevent excessive refinement or coarsening in a single adaptive step, we prescribe that the new element size be no smaller than half the previous element size and no greater than twice the previous element size.

$$\frac{1}{2} \leq \frac{h^e_{\text{new}}}{h^e} \leq 2 \tag{48}$$

6. Results

In this section, we investigate output-based error estimation and mesh adaptation as applied to a model scalar, steady state advection diffusion problem, defined by the linear operator

$$\mathcal{L} := -\kappa \nabla^2 + \boldsymbol{a} \cdot \nabla. \tag{49}$$

Here, κ is a coefficient corresponding to the diffusivity strength and $\boldsymbol{a}$ is a coefficient corresponding to the advective transport. The adjoint operator is readily found (see Appendix B) to be

$$\mathcal{L}^* = -\kappa \nabla^2 - \boldsymbol{a} \cdot \nabla, \tag{50}$$

which is simply another advection-diffusion operator with the advective direction opposite that of the original operator. The bilinear form $A(\cdot, \cdot)$ associated with the operator $\mathcal{L}$ is given as

$$A(v, u) = (\nabla v, \kappa \nabla u) + (v, \boldsymbol{a} \cdot \nabla u) \tag{51}$$

where $(\cdot, \cdot)$ denotes the L_2 inner product.

The mesh Peclét number α is given by $\alpha := \frac{h|\boldsymbol{a}|}{2\kappa}$, where $h = \text{meas}(\Omega^e)$ is a characteristic measure of the mesh element size. In one dimension, the stabilization parameter τ^e is given [16] as:

$$\tau^e = \frac{h}{2|\boldsymbol{a}|}(\coth \alpha + \frac{1}{\alpha}) \tag{52}$$

The parameter τ^e exactly solves (13) in one spatial dimension, but we emphasize that utilizing this parameter in two spatial dimensions introduces yet another approximation to the fine-scale solution.

For a chosen functional output quantity $J(u)$, the *effectivity index* is defined as

$$I = \frac{J(u) - J(u^h)}{\eta}, \tag{53}$$

the ratio of the exact error to the estimated error. The effectivity index provides a measure of the degree to which the error is underestimated. An effectivity index of $I = 1$ is desirable, as it indicates the error estimate has exactly recovered the error.

For each numerical example, the primal and dual problems are solved using the same finite element discretization. That is the same finite element basis functions and the same finite element mesh are used to solve the primal and dual problems. The mesh used in each example consists of simplical elements in one or two dimensions, and the finite element subspace $\mathcal{V}^h$ is defined by piecewise linear Lagrange shape functions. The primal problem is given by equation (20) and the dual problem is given by equation (34), where we emphasize that homogeneous Dirichlet boundary conditions are applied to both the primal and dual problems. Finally, we note that we have provided Appendix C to concretely demonstrate the propositions derived in Section 4.

6.1. One dimensional example

Let $\Omega = \{x : x \in [0,1]\}$. We choose the forcing function for the primal to be $f = 1$, and the functional quantity of interest $J(u) = \int_\Omega u \, \mathrm{d}\Omega$, such that $q = 1$ for the dual problem. The diffusivity coefficient is chosen to be $\kappa = 0.001$ and the advective coefficient $a = 1$. The exact solution to the primal PDE (1) is

$$u(x) = \frac{1}{a}\left(x - \frac{\exp(\frac{ax}{\kappa}) - 1}{\exp(\frac{a}{\kappa}) - 1}\right) \tag{54}$$

and the exact value for the chosen quantity of interest is $J(u) = 0.499$.

We investigate the accuracy of the error estimate obtained by $\eta = \eta_1 = \eta_2$. Table 1 shows the computed functional quantity of interest and the effectivity indices for the one-dimensional problem solved on meshes with n_{el} elements with mesh size $h = \frac{1}{n_{el}}$. For each chosen mesh size, the effectivity index is exactly one meaning the error estimate η exactly recovers the output error. It is well known (*c.f.* [16]) that our choice of τ^e results in a solution u^h that is nodally exact. For this reason, it is unsurprising that the output error is exactly recovered for this example.

n_{el}	α	$J(u^h)$	I
10	5.000e+01	4.5000e-01	1.000
20	2.500e+01	4.7500e-01	1.000
40	1.250e+01	4.8750e-01	1.000
80	6.250e+00	4.9375e-01	1.000
160	3.125e+00	4.9686e-01	1.000

Table 1: Effectivity indices for a 1D advection- diffusion example with a global QoI

6.2. A manufactured solution

Let $\Omega = \{\boldsymbol{x} : \boldsymbol{x} \in [0,1] \times [0,1]\}$. Let $\boldsymbol{e_i}$ and $\boldsymbol{e_j}$ be unitary vectors in the x and y directions, respectively. We choose the advective coefficient to be $\boldsymbol{a} = \boldsymbol{e_i} + \boldsymbol{e_j}$, the diffusive coefficient to be $\kappa = 0.001$, and the forcing function f such that the exact solution is given by

$$u(x, y) = \sin(\pi x)\sin(\pi y). \tag{55}$$

The quantity of interest is chosen to be $J(u) = \int_\Omega u \, \mathrm{d}\Omega$, such that the dual forcing function is $q = 1$. The exact value of the quantity of interest is $J(u) = \frac{1}{\pi^2} \approx .405284$. Again, we investigate the effectivity of the error estimate $\eta = \eta_1 = \eta_2$ for meshes with uniformly n_{el} uniformly distributed triangular elements. Table 2 shows effectivity indices obtained for various meshes. As the mesh size decreases and the number of elements increases, the effectivity index tends to one.

6.3. Advection in an L-shaped domain

Let $\Omega = \{\boldsymbol{x} : \boldsymbol{x} \in [0,1] \times [0,1] \cup [0,1] \times [-1,0] \cup [-1,0] \times [0,1]\}$. Let $\boldsymbol{e_i}$ and $\boldsymbol{e_j}$ be unitary vectors in the x and y direction, respectively. We choose the advective coefficient to be $\boldsymbol{a} = -\boldsymbol{e_i} + \boldsymbol{e_j}$, the diffusive

n_{el}	$J(u^h)$	I
200	4.0493e-01	1.083
800	4.0512e-01	1.023
3200	4.0521e-01	1.009
12800	4.0525e-01	1.004
51200	4.0527e-01	1.001

Table 2: Effectivity indices for a 2D advection- diffusion example with a global QoI

coefficient to be $\kappa = 0.001$, and the forcing function $f = 1$. We investigate adaptivity for two output quantities: $J_1(u) = \int_\Omega u \, \mathrm{d}\Omega$ and $J_2(u) = \int_\Omega q_2 u \, \mathrm{d}\Omega$, where q_2 is defined as

$$q_2 := \begin{cases} 1 & \text{if } -0.95 \leq x \leq -0.5 \text{ and } 0.5 \leq y \leq 0.95 \\ 0 & \text{otherwise} \end{cases} \tag{56}$$

That is, q_2 samples the solution u^h on a square patch in the upper right corner of the domain Ω. The primal solution u^h and the dual solutions corresponding to the two quantities of interest are shown in Figure 1. Note that the primal solution contains steep gradients at the two left-most surfaces and the upper surface of the L-shaped domain.

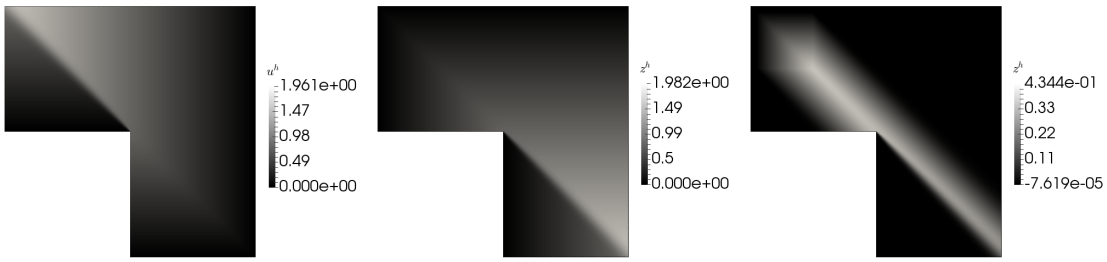

Figure 1: The primal solution u^h (left) and the dual solutions z^h corresponding to $J_1(u)$ (center) and $J_2(u)$ (right)

We investigate the ability of four adaptive schemes to accurately assess the two functional quantities. Each scheme proceeds by iteratively performing the steps

Solve primal PDE $\rightarrow$ Localize error $\rightarrow$ Adapt mesh.

The first adaptive scheme, referred to as UNIF, remeshes the entire domain with a uniform size field. For the two output quantities, errors are computed for the meshes generated with the mesh sizes $h = \{\frac{1}{4}, \frac{1}{8}, \frac{1}{16}, \frac{1}{32}, \frac{1}{64}\}$. In principle, the step to localize the error is not required for this scheme.

For comparison to more traditional energy-based methods, the second adaptive scheme is chosen based on a Zienkiewicz-Zhu type error estimate [27] [28], whereby error indicators are computed as the difference between solution gradients ∇u^h that are discontinuous between elements and a nodally smoothed approximation to the gradient $(\nabla u^h)^*$ that is obtained via a least-squares fit over a patch of elements. Once error indicators are computed, the size field is set according to the size field equation (47) such that the target number of elements N is twice the number of elements in the previous mesh. We refer to this scheme as the superconvergent patch recovery (SPR) adaptive scheme.

The third and fourth adaptive schemes are based on the error indicators η_1^e and η_2^e, respectively, and are referred to as the VMS1 and VMS2 adaptive schemes, respectively. Again, once the error indicators have been computed, the size field is set according to the size field equation (47) such that the target number of elements N is twice the number of elements in the previous mesh. We note that the scheme VMS2 is the

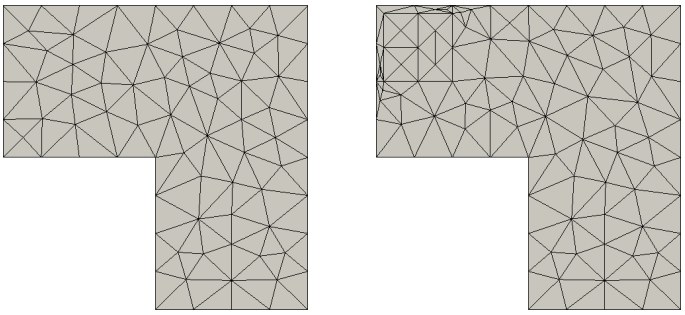

Figure 2: Initial meshes for the outputs $J_1(u)$ (left) and $J_2(u)$ (right)

only one which necessitates the solution of the dual PDE model, which is implicitly included in the 'Localize error' step.

For each quantity of interest, an initial mesh with a uniform size of $h = \frac{1}{4}$ was generated as shown in Figure 2. From this initial mesh, each adaptive scheme was run until meshes with over $10,000$ degrees of freedom were produced. The exact values of the two output quantities were computed on 'truth' meshes, which are finer at every spatial location in the domain when compared to the meshes obtained via the four adaptive schemes. The values of the quantities of interest were found to be $J_1(u) = 1.6588688371$ and $J_2(u) = 0.23109653499$.

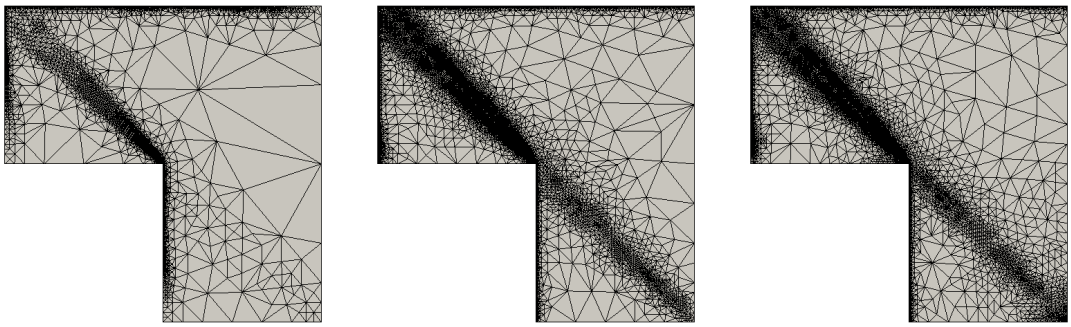

Figure 3: Final adapted meshes for the output $J_1(u)$ using the SPR (left), VMS1 (center), and VMS2 (right) adaptive schemes

Figure 3 shows the meshes obtained at the final iteration of the SPR, VMS1, and VMS2 adaptive schemes for the global output quantity $J_1(u)$. As expected, the SPR scheme strongly refines the mesh in areas where the gradient changes drastically. These areas include the left-most and upper-most surfaces of the L-shaped domain where boundary layers in the solution exist, as well as the diagonal downstream of the reentrant corner where there is a sudden change in the solution magnitude. In addition to performing mesh refinement in the areas that the SPR scheme targets, the VMS1 and VMS2 also refine the mesh along the diagonal upstream of the reentrant corner to accurately resolve features of the dual solution z^h. For the global quantity $J_1(u)$, the VMS1 and VMS2 schemes yield final meshes with very similar characteristics. At each iteration in the adaptive schemes, the output error $|J_1(u) - J_1(u^h)|$ was computed. Figure 4 displays the convergence histories for each adaptive scheme. Unsurprisingly, the VMS1 and VMS2 adaptive schemes compute the output error more accurately than the SPR and UNIF with a comparable number of degrees of freedom.

Figure 5 displays the output meshes at the final iteration of the SPR, VMS1, and VMS2 adaptive schemes for the local output quantity $J_2(u)$. Again, it is clear that the SPR strongly refines the mesh

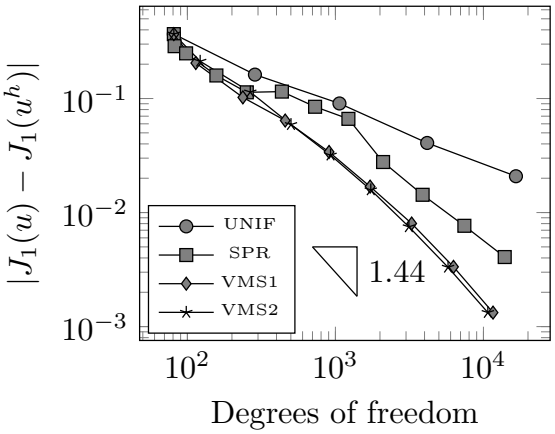

Figure 4: Convergence history for various adaptive schemes for the output $J_1(u)$.

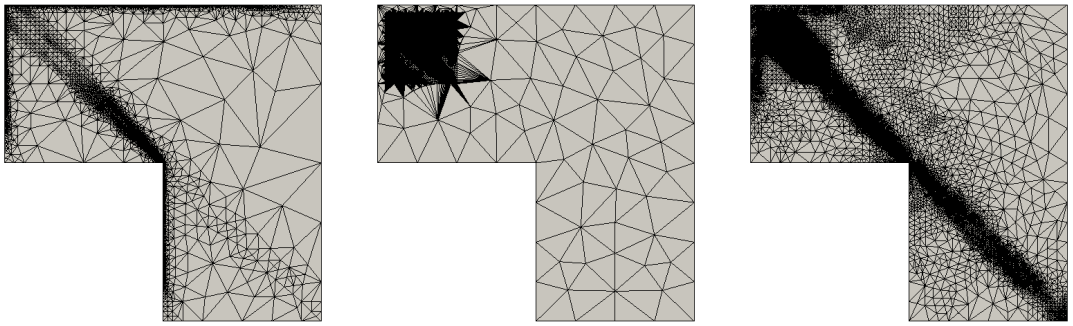

Figure 5: Final adapted meshes for the output $J_2(u)$ using the SPR (left), VMS1 (center), and VMS2 (right) adaptive schemes

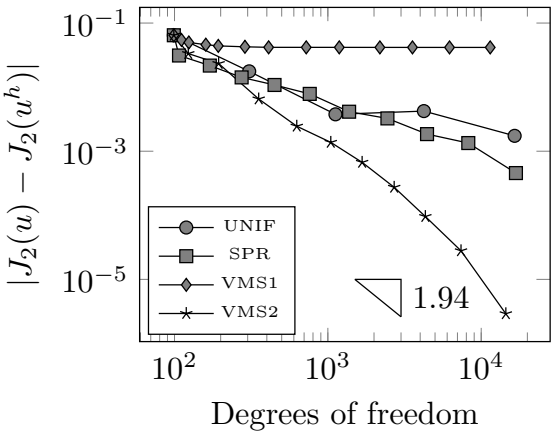

Figure 6: Convergence history for various adaptive schemes for the output $J_2(u)$.

in areas where the gradient changes drastically. The VMS1 scheme only performs mesh refinement over the square subdomain over which q_2 is non-zero and does not seek accurately resolve the mesh to capture features of the primal or dual solutions. In contrast, the VMS2 strongly refines the mesh over the square subdomain of interest, while also resolving areas upstream of the domain to accurately account for the features of the primal and dual solutions. For the output quantity $J_2(u)$, convergence histories for each adaptive scheme are shown in Figure 6. It is clear from both the convergence diagram and final adapted mesh for the VMS1 scheme that the VMS1 scheme is completely insufficient to drive mesh adaptation for a locally defined output quantity. On the other hand, the VMS2 adaptive scheme is able to compute the ouptut quantity with much greater accuracy than the UNIF and SPR schemes when using a comparable number of degrees of freedom.

7. Conclusions

For VMS methods, we have proposed a novel approach to enriching the dual solution for duality-based functional error estimation using VMS techniques. We have demonstrated the utility of this technique to drive mesh adaptation to accurately compute output quantities.

Future work includes investigating the effect of choosing different optimality conditions $\phi(\cdot)$ and $\phi_d(\cdot)$ for the primal and dual problems, respectively, extending error estimates to account for nonlinearities in both the PDE model and in the functional output quantity, investigating the effect of utilizing more accurate approximations to the fine-scale primal and dual solutions, and extending the arguments presented to a mixture of non-homogeneous Dirichlet and Nuemann boundary conditions.

References

[1] Mark Ainsworth and J Tinsley Oden. A posteriori error estimation in finite element analysis, 2011.

[2] Frédéric Alauzet, Xiangrong Li, E Seegyoung Seol, and Mark S Shephard. Parallel anisotropic 3d mesh adaptation by mesh modification. *Engineering with Computers*, 21(3):247–258, 2006.

[3] Wolfgang Bangerth and Rolf Rannacher. *Adaptive finite element methods for differential equations*. Birkhäuser, 2013.

[4] Teri Barth, Pavel Bochev, Max Gunzburger, and John Shadid. A taxonomy of consistently stabilized finite element methods for the stokes problem. *SIAM Journal on Scientific Computing*, 25(5):1585–1607, 2004.

[5] Roland Becker and Rolf Rannacher. An optimal control approach to a posteriori error estimation in finite element methods. *Acta Numerica 2001*, 10:1–102, 2001.

[6] Ramzy Boussetta, Thierry Coupez, and Lionel Fourment. Adaptive remeshing based on a posteriori error estimation for forging simulation. *Computer methods in applied mechanics and engineering*, 195(48):6626–6645, 2006.

[7] Alexander N Brooks and Thomas JR Hughes. Streamline upwind/petrov-galerkin formulations for convection dominated flows with particular emphasis on the incompressible navier-stokes equations. *Computer methods in applied mechanics and engineering*, 32(1):199–259, 1982.

[8] Eric C Cyr, John Shadid, and Tim Wildey. Approaches for adjoint-based a posteriori analysis of stabilized finite element methods. *SIAM Journal on Scientific Computing*, 36(2):A766–A791, 2014.

[9] Kenneth Eriksson, Don Estep, Peter Hansbo, and Claes Johnson. Introduction to adaptive methods for differential equations. *Acta numerica*, 4:105–158, 1995.

[10] Krzysztof J Fidkowski and David L Darmofal. Review of output-based error estimation and mesh adaptation in computational fluid dynamics. *AIAA journal*, 49(4):673–694, 2011.

[11] Leopoldo P Franca and Sérgio L Frey. Stabilized finite element methods: Ii. the incompressible navier-stokes equations. *Computer Methods in Applied Mechanics and Engineering*, 99(2-3):209–233, 1992.

[12] Leopoldo P Franca, Sergio L Frey, and Thomas JR Hughes. Stabilized finite element methods: I. application to the advective-diffusive model. *Computer Methods in Applied Mechanics and Engineering*, 95(2):253–276, 1992.

[13] Guillermo Hauke, Mohamed H Doweidar, and Mario Miana. The multiscale approach to error estimation and adaptivity. *Computer Methods in Applied Mechanics and Engineering*, 195(13):1573–1593, 2006.

[14] Guillermo Hauke and Daniel Fuster. Variational multiscale a posteriori error estimation for quantities of interest. *Journal of Applied Mechanics*, 76(2):021201, 2009.

[15] Guillermo Hauke, Daniel Fuster, and Mohamed H Doweidar. Variational multiscale a-posteriori error estimation for multi-dimensional transport problems. *Computer Methods in Applied Mechanics and Engineering*, 197(33):2701–2718, 2008.

[16] Thomas JR Hughes, Gonzalo R Feijóo, Luca Mazzei, and Jean-Baptiste Quincy. The variational multiscale method : a paradigm for computational mechanics. *Computer methods in applied mechanics and engineering*, 166(1):3–24, 1998.

[17] Thomas JR Hughes, Leopoldo P Franca, and Marc Balestra. A new finite element formulation for computational fluid dynamics: V. circumventing the babuška-brezzi condition: A stable petrov-galerkin formulation of the stokes problem accommodating equal-order interpolations. *Computer Methods in Applied Mechanics and Engineering*, 59(1):85–99, 1986.

[18] Thomas JR Hughes, Leopoldo P Franca, and Gregory M Hulbert. A new finite element formulation for computational fluid dynamics: VIII. the galerkin/least-squares method for advective-diffusive equations. *Computer Methods in Applied Mechanics and Engineering*, 73(2):173–189, 1989.
[19] Thomas JR Hughes and Giancarlo Sangalli. Variational multiscale analysis: the fine-scale green's function, projection, optimization, localization, and stabilized methods. *SIAM Journal on Numerical Analysis*, 45(2):539–557, 2007.
[20] Daniel A Ibanez, E Seegyoung Seol, Cameron W Smith, and Mark S Shephard. Pumi: Parallel unstructured mesh infrastructure. *ACM Transactions on Mathematical Software (TOMS)*, 42(3):17, 2016.
[21] Mats G Larson and Axel Målqvist. Adaptive variational multiscale methods based on a posteriori error estimation: energy norm estimates for elliptic problems. *Computer methods in applied mechanics and engineering*, 196(21):2313–2324, 2007.
[22] Xiangrong Li, Mark S Shephard, and Mark W Beall. 3d anisotropic mesh adaptation by mesh modification. *Computer methods in applied mechanics and engineering*, 194(48):4915–4950, 2005.
[23] Arif Masud and Timothy J Truster. A framework for residual-based stabilization of incompressible finite elasticity: stabilized formulations and methods for linear triangles and tetrahedra. *Computer Methods in Applied Mechanics and Engineering*, 267:359–399, 2013.
[24] Arif Masud, Timothy J Truster, and Lawrence A Bergman. A variational multiscale a posteriori error estimation method for mixed form of nearly incompressible elasticity. *Computer Methods in Applied Mechanics and Engineering*, 200(47):3453–3481, 2011.
[25] Assad A Oberai and Peter M Pinsky. A multiscale finite element method for the helmholtz equation. *Computer Methods in Applied Mechanics and Engineering*, 154(3):281–297, 1998.
[26] Tayfun E Tezduyar, Sanjay Mittal, SE Ray, and R Shih. Incompressible flow computations with stabilized bilinear and linear equal-order-interpolation velocity-pressure elements. *Computer Methods in Applied Mechanics and Engineering*, 95(2):221–242, 1992.
[27] Olgierd Cecil Zienkiewicz and Jian Zhong Zhu. The superconvergent patch recovery and a posteriori error estimates. Part 1: The recovery technique. *International Journal for Numerical Methods in Engineering*, 33(7):1331–1364, 1992.
[28] Olgierd Cecil Zienkiewicz and Jian Zhong Zhu. The superconvergent patch recovery and a posteriori error estimates. part 2: Error estimates and adaptivity. *International Journal for Numerical Methods in Engineering*, 33(7):1365–1382, 1992.

Appendix A. Non-homogeneous boundary conditions

Extensions to non-homogeneous Dirichlet boundary conditions for the primal model, given as

$$\begin{cases} \mathcal{L}u = f, & \boldsymbol{x} \in \Omega, \\ u = g, & \boldsymbol{x} \in \partial\Omega, \end{cases} \tag{A.1}$$

can readily be made by introducing the decomposition $u = u_0 + \widetilde{g}$, where $\mathrm{tr}(\widetilde{g}) = g$. The problem is then reposed as a homogeneous Dirichlet problem given by

$$\begin{cases} \mathcal{L}u_0 = f + \mathcal{L}\widetilde{g}, & \boldsymbol{x} \in \Omega, \\ u_0 = 0, & \boldsymbol{x} \in \partial\Omega, \end{cases} \tag{A.2}$$

where all arguments made previously can be applied to this modified formulation, provided $f + \mathcal{L}\widetilde{g} \in \mathcal{V}^*$.

Extensions to non-homogeneous Neumann boundary conditions require additional investigation. To proceed, consider the primal problem given as

$$\begin{cases} \mathcal{L}u = f & \boldsymbol{x} \in \Omega, \\ u = 0, & \boldsymbol{x} \in \partial\Omega_D \\ Bu = h & \boldsymbol{x} \in \partial\Omega_N, \end{cases} \tag{A.3}$$

where $\Omega_D \cup \Omega_N = \Omega$ and $\Omega_D \cap \Omega_N = \{\varnothing\}$. Multiplying the left hand side of the primal problem (A.3) by an arbitrary test function v and integrating by parts over the domain twice yields the relationship

$$\int_\Omega v\mathcal{L}u \,\mathrm{d}\Omega + \int_{\partial\Omega_N} vBu \,\mathrm{d}\Gamma = \int_\Omega \mathcal{L}^* vu \,\mathrm{d}\Omega + \int_{\partial\Omega_N} B^* vu \,\mathrm{d}\Gamma. \tag{A.4}$$

All subsequent derivations would need to be made considering this relationship, which involves the boundary operator B, rather than relationship (9) which has been used extensively in this paper.

Appendix B. Derivation of the advection-diffusion adjoint operator

Let $\mathcal{L} : \mathcal{V} \to \mathcal{V}^*$ be the steady-state, constant coefficient operator utilized in section 6:

$$\mathcal{L}u := -\kappa\nabla^2 u + \boldsymbol{a} \cdot \nabla u \tag{B.1}$$

such that $\mathcal{V} = H_0^1(\Omega)$ and $\mathcal{V}^* = H^{-1}(\Omega)$. To determine the corresponding operator: $\mathcal{L}^*$ that satisfies the adjoint property:

$${}_{\mathcal{V}^*}\langle z, \mathcal{L}u\rangle_{\mathcal{V}} = {}_{\mathcal{V}}\langle \mathcal{L}^* z, u\rangle_{\mathcal{V}^*} \quad \forall\, u, z \in H_0^1(\Omega), \tag{B.2}$$

we multiply $\mathcal{L}u$ by an arbitrary function $z \in H_0^1(\Omega)$ and repeatedly apply the divergence theorem. This proceeds as follows:

$$\begin{aligned}
{}_{\mathcal{V}}\langle z, \mathcal{L}u\rangle_{\mathcal{V}^*} &= \int_\Omega z(-\kappa\nabla^2 u + \boldsymbol{a} \cdot \nabla u)\,\mathrm{d}\Omega \\
&= -\int_\Omega z\kappa\nabla^2 u\,\mathrm{d}\Omega + \int_\Omega z\boldsymbol{a} \cdot \nabla u\,\mathrm{d}\Omega \\
&= -\int_{\partial\Omega} z\kappa\nabla u \cdot \boldsymbol{n}\,\mathrm{d}\Gamma + \int_\Omega \kappa\nabla z \cdot \nabla u\,\mathrm{d}\Omega + \int_{\partial\Omega} (z\boldsymbol{a}u) \cdot \boldsymbol{n}\,\mathrm{d}\Gamma - \int_\Omega \boldsymbol{a} \cdot \nabla z u\,\mathrm{d}\Omega \\
&= \int_\Omega \kappa\nabla z \cdot \nabla u\,\mathrm{d}\Omega - \int_\Omega \boldsymbol{a} \cdot \nabla z u\,\mathrm{d}\Omega \\
&= \int_{\partial\Omega} (\kappa\nabla z u) \cdot \boldsymbol{n}\,\mathrm{d}\Gamma - \int_\Omega \kappa\nabla^2 z u\,\mathrm{d}\Omega - \int_\Omega \boldsymbol{a} \cdot \nabla z u\,\mathrm{d}\Omega \\
&= -\int_\Omega \kappa\nabla^2 z u\,\mathrm{d}\Omega - \int_\Omega \boldsymbol{a} \cdot \nabla z u\,\mathrm{d}\Omega \\
&= \int_\Omega (-\kappa\nabla^2 z - \boldsymbol{a} \cdot \nabla z) u\,\mathrm{d}\Omega \\
&= {}_{\mathcal{V}^*}\langle \mathcal{L}^* z, u\rangle_{\mathcal{V}}
\end{aligned}$$

Here the third equality is achieved by application of the divergence theorem to both terms, the fourth equality holds since $z \in H_0^1(\Omega)$, the fifth equality is achieved by application of the divergence theorem to the leftmost term, and the sixth equality holds since $u \in H_0^1(\Omega)$. Thus, the operator $\mathcal{L}^* : H_0^1(\Omega) \to H^{-1}(\Omega)$ is defined as

$$\mathcal{L}^* z := -\kappa\nabla^2 z - \boldsymbol{a} \cdot \nabla z. \tag{B.3}$$

We make the observation that there has been a sign change for the advective term since the operator $\mathcal{L}$ is not self-adjoint. This sign change, however, is absorbed in the definition of the operator $\mathcal{L}^*$ and in no way introduces a sign change in the fundamental property:

$${}_{\mathcal{V}}\langle z, \mathcal{L}u\rangle_{\mathcal{V}^*} = {}_{\mathcal{V}^*}\langle \mathcal{L}^* z, u\rangle_{\mathcal{V}} \quad \forall\, u, z \in H_0^1(\Omega). \tag{B.4}$$

Appendix C. Propositions applied to the advection-diffusion operator

We restate the adjoint property (B.4) as

$$\int_\Omega z(-\kappa\nabla^2 u + \boldsymbol{a} \cdot \nabla u)\,\mathrm{d}\Omega = \int_\Omega (-\kappa\nabla^2 z - \boldsymbol{a} \cdot \nabla z) u\,\mathrm{d}\Omega \quad \forall\, u, z \in H_0^1(\Omega) \tag{C.1}$$

We now define the primal problem as:

$$\begin{cases} -\kappa\nabla^2 u + \boldsymbol{a} \cdot \nabla u = f, & \boldsymbol{x} \in \Omega, \\ u = 0, & \boldsymbol{x} \in \partial\Omega, \end{cases} \tag{C.2}$$

corresponding to equation (1), where $f \in H^{-1}(\Omega)$. We note that the primal residual operator is given as:

$$\mathcal{R}u := f + \kappa\nabla^2 u - \boldsymbol{a}\cdot\nabla u. \tag{C.3}$$

We define the continuous variational multiscale formulation of the primal problem as: find $\overline{u} \in \overline{\mathcal{V}}$ such that

$$\int_\Omega (-\kappa\nabla^2\overline{v} - \boldsymbol{a}\cdot\nabla\overline{v})\mathcal{G}'\mathcal{R}\overline{u}\,\mathrm{d}\Omega = \int_\Omega \overline{v}\mathcal{R}\overline{u}\,\mathrm{d}\Omega \quad \forall\,\overline{v} \in H_0^1(\Omega), \tag{C.4}$$

corresponding to equation (11), where we leave the fine-scale Green's operator $\mathcal{G}' : H^{-1}(\Omega) \to H_0^1(\Omega)$ as an unspecified abstract operator. Here we note that $\mathcal{G}'\mathcal{R}\overline{u} \in H_0^1(\Omega)$. Let $\mathcal{V}^h \subset \mathcal{V}$ denote a classical finite element space consisting of piecewise linear functions defined over a discretization of the domain Ω. The primal subgrid model can then be stated as: find $u^h \in \mathcal{V}^h$ such that

$$\sum_{e=1}^{n_{el}} \int_{\Omega^e} (-\kappa\nabla^2 v^h - \boldsymbol{a}\cdot\nabla v^h)(\tau^e\mathcal{R}u^h)\,\mathrm{d}\Omega = \int_\Omega v^h\mathcal{R}u^h\,\mathrm{d}\Omega \quad \forall\, v^h \in \mathcal{V}^h, \tag{C.5}$$

corresponding to equation (15), where we leave τ^e unspecified.

We define the dual problem as:

$$\begin{cases} -\kappa\nabla^2 z - \boldsymbol{a}\cdot\nabla z = q, & \boldsymbol{x} \in \Omega, \\ \qquad\qquad\qquad z = 0, & \boldsymbol{x} \in \partial\Omega, \end{cases} \tag{C.6}$$

corresponding to equation (23), where $q \in H^{-1}(\Omega)$. We note that the dual residual operator is given as:

$$\mathcal{R}^* z := q + \kappa\nabla^2 z + \boldsymbol{a}\cdot\nabla z. \tag{C.7}$$

We define the continuous variational multiscale formulation of the dual problem as: find $\overline{z} \in \overline{\mathcal{V}}$ such that

$$\int_\Omega \mathcal{G}_d'\mathcal{R}^*\overline{z}(-\kappa\nabla^2\overline{v} + \boldsymbol{a}\cdot\nabla\overline{v})\,\mathrm{d}\Omega = \int_\Omega \mathcal{R}^*\overline{z}\overline{v}\,\mathrm{d}\Omega \quad \forall\,\overline{v} \in H_0^1(\Omega), \tag{C.8}$$

corresponding to equation (27), where again we leave the dual fine-scale Green's operator $\mathcal{G}_d' : H^{-1}(\Omega) \to H_0^1(\Omega)$ unspecified. We note that $\mathcal{G}_d'\mathcal{R}^*\overline{z} \in H_0^1(\Omega)$ The dual subgrid model can then be stated as: find $z^h \in \mathcal{V}^h$ such that

$$\sum_{e=1}^{n_{el}} \int_{\Omega^e} (\tau_d^e\mathcal{R}^* z^h)(-\kappa\nabla^2 v^h + \boldsymbol{a}\cdot\nabla v^h)\,\mathrm{d}\Omega = \int_\Omega \mathcal{R}^* z^h v^h\,\mathrm{d}\Omega \quad \forall\, v^h \in \mathcal{V}^h, \tag{C.9}$$

corresponding to equation (31), where we leave τ_d^e unspecified.

Appendix C.1. Proposition 2

For any solutions $u = u' + \overline{u}$ to the continuous VMS formulation (C.4) and $z = z' + \overline{z}$ to the continuous dual VMS formulation (C.8), we derive the error representation:

$$\begin{aligned}
J(u) - J(\overline{u}) &= \int_\Omega qu \,\mathrm{d}\Omega - \int_\Omega q\overline{u} \,\mathrm{d}\Omega \\
&= \int_\Omega (-\kappa\nabla^2 z - \boldsymbol{a}\cdot\nabla z)u \,\mathrm{d}\Omega - \int_\Omega (-\kappa\nabla^2 z - \boldsymbol{a}\cdot\nabla z)\overline{u} \,\mathrm{d}\Omega \\
&= \int_\Omega z(-\kappa\nabla^2 u + \boldsymbol{a}\cdot\nabla u) \,\mathrm{d}\Omega - \int_\Omega z(-\kappa\nabla^2 \overline{u} + \boldsymbol{a}\cdot\nabla \overline{u}) \,\mathrm{d}\Omega \\
&= \int_\Omega zf \,\mathrm{d}\Omega - \int_\Omega z(-\kappa\nabla^2 \overline{u} + \boldsymbol{a}\cdot\nabla \overline{u}) \,\mathrm{d}\Omega \\
&= \int_\Omega z\mathcal{R}\overline{u} \,\mathrm{d}\Omega \\
&= \int_\Omega z'\mathcal{R}\overline{u} \,\mathrm{d}\Omega + \int_\Omega \overline{z}\mathcal{R}\overline{u} \,\mathrm{d}\Omega \\
&= \int_\Omega z'\mathcal{R}\overline{u} \,\mathrm{d}\Omega + \int_\Omega (-\kappa\nabla^2 \overline{z} - \boldsymbol{a}\cdot\nabla \overline{z})\mathcal{G}'\mathcal{R}\overline{u} \,\mathrm{d}\Omega \\
&= \int_\Omega (\mathcal{G}_d'\mathcal{R}^*\overline{z})\mathcal{R}\overline{u} \,\mathrm{d}\Omega + \int_\Omega (-\kappa\nabla^2 \overline{z} - \boldsymbol{a}\cdot\nabla \overline{z})\mathcal{G}'\mathcal{R}\overline{u} \,\mathrm{d}\Omega \\
&= {}_{\mathcal{V}}\langle \mathcal{G}_d'\mathcal{R}^*\overline{z}, \mathcal{R}\overline{u}\rangle_{\mathcal{V}^*} + {}_{\mathcal{V}^*}\langle \mathcal{L}^*\overline{z}, \mathcal{G}'\mathcal{R}\overline{u}\rangle_{\mathcal{V}}
\end{aligned}$$

Here the first equality is by definition (21), the second equality is due to the dual PDE (C.6), the third equality is due to the fundamental relation (C.1), the fourth equality is due to the primal PDE (C.2), the fifth equality is due to the definition of the primal residual (C.3), the sixth equality is due to the sum decomposition of the dual solution $z = z' + \overline{z}$, the seventh equality is due to the continuous variational formulation of the primal problem (C.4), the eight equality is due to the definition of the fine-scale dual solution (24), and the ninth equality is due to the definition of the duality pairing we have chosen.

Appendix C.2. Proposition 4

For any solutions u to the primal model (2), z to the dual model (22), u^h to the primal subgrid model (14) and z^h to the dual subgrid model (30), we derive the error representation

$$\begin{aligned}
J(u) - J(u^h) &= \int_\Omega qu \,\mathrm{d}\Omega - \int_\Omega qu^h \,\mathrm{d}\Omega \\
&= \int_\Omega (-\kappa\nabla^2 z - \boldsymbol{a}\cdot\nabla z)u \,\mathrm{d}\Omega - \int_\Omega (-\kappa\nabla^2 z - \boldsymbol{a}\cdot\nabla z)u^h \,\mathrm{d}\Omega \\
&= \int_\Omega z(-\kappa\nabla^2 u + \boldsymbol{a}\cdot\nabla u) \,\mathrm{d}\Omega - \int_\Omega z(-\kappa\nabla^2 u^h + \boldsymbol{a}\cdot\nabla u^h) \,\mathrm{d}\Omega \\
&= \int_\Omega zf \,\mathrm{d}\Omega - \int_\Omega z(-\kappa\nabla^2 u^h + \boldsymbol{a}\cdot\nabla u^h) \,\mathrm{d}\Omega \\
&= \int_\Omega z\mathcal{R}u^h \,\mathrm{d}\Omega \\
&= \int_\Omega z\mathcal{R}u^h \,\mathrm{d}\Omega - \int_\Omega z^h\mathcal{R}u^h \,\mathrm{d}\Omega + \sum_{e=1}^{n_{el}} \int_\Omega (-\kappa\nabla^2 z^h - \boldsymbol{a}\cdot\nabla z^h)(\tau^e\mathcal{R}u^h) \,\mathrm{d}\Omega \\
&= \int_\Omega (z - z^h)\mathcal{R}u^h + \sum_{e=1}^{n_{el}} \int_\Omega (-\kappa\nabla^2 z^h - \boldsymbol{a}\cdot\nabla z^h)(\tau^e\mathcal{R}u^h) \,\mathrm{d}\Omega \\
&= \int_\Omega (\widetilde{z}' + \widetilde{z})\mathcal{R}u^h + \sum_{e=1}^{n_{el}} \int_\Omega (-\kappa\nabla^2 z^h - \boldsymbol{a}\cdot\nabla z^h)(\tau^e\mathcal{R}u^h) \,\mathrm{d}\Omega \\
&= \int_\Omega \widetilde{z}'\mathcal{R}u^h + \sum_{e=1}^{n_{el}} \int_\Omega (-\kappa\nabla^2 z^h - \boldsymbol{a}\cdot\nabla z^h)(\tau^e\mathcal{R}u^h) \,\mathrm{d}\Omega + \int_\Omega \widetilde{z}\mathcal{R}u^h \\
&= \int_\Omega (\tau_d^e\mathcal{R}^* z^h)\mathcal{R}u^h + \sum_{e=1}^{n_{el}} \int_\Omega (-\kappa\nabla^2 z^h - \boldsymbol{a}\cdot\nabla z^h)(\tau^e\mathcal{R}u^h) \,\mathrm{d}\Omega + \int_\Omega \widetilde{z}\mathcal{R}u^h
\end{aligned}$$

where the first equality is by definition (21), the second equality is due to the dual PDE (C.6), the third equality is due to the fundamental relationship (C.1), the fourth equality is due to the primal PDE (C.2), the fifth equality is due to the definition of the primal residual (C.3), the sixth equality is due to the primal subgrid model (C.5) (where we have added and subtracted equal terms), the seventh equality is due to linearity, the eighth equality is due to the decomposition of the dual solution (19), the ninth equality is due to linearity, and the tenth equality is due to the fine-scale approximation to the dual solution (32).

Appendix C.3. Proposition 5

We first note that the derivation in Appendix B can be carried out in exactly the same manner for $u, z \in H_0^1(\Omega^e)$ to obtain the result:

$$\int_{\Omega^e} z(-\kappa\nabla^2 u + \boldsymbol{a}\cdot\nabla u) \,\mathrm{d}\Omega = \int_{\Omega^e} (-\kappa\nabla^2 z - \boldsymbol{a}\cdot\nabla z)u \,\mathrm{d}\Omega \quad \forall\, u, z \in H_0^1(\Omega^e) \tag{C.10}$$

We note that the problem (12) defining the primal element-level Green's function implies that $g^e(\boldsymbol{x};\boldsymbol{y}) \in H_0^1(\Omega^e)$. Similarly, the dual element-level Green's function satisfies $g_d^e(\boldsymbol{x};\boldsymbol{y}) \in H_0^1(\Omega^e)$ from equation (28). With this information, we utilize the relationship (C.10) to verify that $g^e(\boldsymbol{x};\boldsymbol{y}) = g_d^e(\boldsymbol{x};\boldsymbol{y})$, even though the

operator $\mathcal{L}$ is not self-adjoint.

$$
\begin{aligned}
-\kappa\nabla^2 g^e(\boldsymbol{x};\boldsymbol{y}) - \boldsymbol{a}\cdot\nabla g^e(\boldsymbol{x};\boldsymbol{y}) &= \delta(\boldsymbol{x}-\boldsymbol{y}) \\
\implies \int_{\Omega^e} g_d^e(\boldsymbol{x};\boldsymbol{z})(-\kappa\nabla^2 g^e(\boldsymbol{x};\boldsymbol{y}) - \boldsymbol{a}\cdot\nabla g^e(\boldsymbol{x};\boldsymbol{y}))\,\mathrm{d}\Omega &= \int_{\Omega^e} g_d^e(\boldsymbol{x};\boldsymbol{z})\delta(\boldsymbol{x}-\boldsymbol{y})\,\mathrm{d}\Omega \\
\implies \int_{\Omega^e} (-\kappa\nabla^2 g_d^e(\boldsymbol{x};\boldsymbol{z}) + \boldsymbol{a}\cdot\nabla g_d^e(\boldsymbol{x};\boldsymbol{z}))g^e(\boldsymbol{x};\boldsymbol{y})\,\mathrm{d}\Omega &= \int_{\Omega^e} g_d^e(\boldsymbol{x};\boldsymbol{z})\delta(\boldsymbol{x}-\boldsymbol{y})\,\mathrm{d}\Omega \\
\implies \int_{\Omega^e} \delta(\boldsymbol{x}-\boldsymbol{z})g^e(\boldsymbol{x};\boldsymbol{y})\,\mathrm{d}\Omega &= \int_{\Omega^e} g_d^e(\boldsymbol{x};\boldsymbol{z})\delta(\boldsymbol{x}-\boldsymbol{y})\,\mathrm{d}\Omega \\
\implies g^e(\boldsymbol{z};\boldsymbol{y}) &= g_d^e(\boldsymbol{y};\boldsymbol{z}),
\end{aligned}
$$

Here the first equality is due to the definition of the primal element-level Green's function (12), the second equality is achieved by multiplying by the dual element-level Green's function and integrating over the element domain, the third equality is due to the fundamental relationship (C.10), and the fourth equality is due to the definition of the dual element-level Green's function (28).